Separating Magnitude Response into Real and Imaginary Parts by Mellin Convolution Filters

VAIRIS SHTRAUSS, ALDIS KALPINSH, ULDIS LOMANOVSKIS
Institute for Material Mechanics
University of Latvia
23 Aizkraukles Street, LV 1006 Riga
LATVIA
strauss@pmi.lv, kalpins@pmi.lv, uldis@latndt.lv

Abstract: - The paper is devoted to the determination of the real and imaginary parts from the magnitude responses for causal linear time-invariant systems having monotonic impulse responses. We demonstrate that the problem can be considered as a special filtering task in the Mellin transform domain having a diffuse magnitude response. The theoretical background is given for the separating the magnitude response into the real and imaginary parts by discrete-time Mellin convolution filters processing geometrically sampled magnitude responses and the appropriate finite impulse response (FIR) filters are designed. To compensate exponential shortening frequency ranges of the real and imaginary parts due to the end-effects of FIR filters processing geometrically sampled magnitude responses, the multiple filtering mode is used, where the sets of the first and last input samples are repeatedly processed by the filters having impulse responses with the shifted origins, which gradually vary the number of coefficients with negative and positive indices on each side of the origin. The performance of the designed filters are evaluated in terms of the accuracy of the generated real and imaginary parts and the noise amplification.

Key-Words: - Magnitude Response, Real Part, Imaginary Part, Mellin Convolution Filter, Diffuse Frequency Response, Geometrically Sampled Data, End-Effects, Multiple Filtering Mode

1 Introduction

The paper is devoted to the problem of the determination of real $J'(\omega)$ and imaginary $J''(\omega)$ parts of frequency response

$$\widetilde{J}(\omega) = J'(\omega) + jJ''(\omega)$$

from the magnitude response

$$|\widetilde{J}(\omega)| = \sqrt{[J'(\omega)]^2 + [J''(\omega)]^2} \qquad (1)$$

for causal linear time-invariant systems having monotonic impulse responses (IRs).

Since the real and imaginary parts of frequency responses for causal physical systems are not wholly independent, but are linked by the Kramers-Kronig (KK) relations [1], it means that the magnitude responses are also consistent. This points to a potent feasibility of separating the magnitude response into the real and imaginary parts by discrete-time signal processing methods [2]. At present, however, no techniques known for the determining the real and imaginary parts from the magnitude response. Nevertheless, development of such techniques are of particular interest, because they may considerably simplify the determination of the real and imaginary parts, thanks to the fact that magnitude responses are relatively easily and accurately measurable signals, for example, by measuring amplitudes of steady-state responses of linear time-invariant systems to harmonic excitations [3-5].

We propose to solve the problem by Mellin convolution filters [6-9] developed for solving interconversion problems between linear monotonic and locally monotonic material functions interrelated by the Mellin convolution transforms (MCT)

$$y(\omega) = \int_0^\infty x(u) k\left(\frac{\omega}{u}\right)\frac{du}{u}, \qquad (2)$$

where $x(.)$ is input function, $y(.)$ is output function, and $k(.)$ is kernel.

Theoretical basis of the Mellin convolution filtering [6-9] comes from the fact that transform (2) for logarithmically transformed variables

$$\omega^* = \log_q \omega/\omega_0 \quad (3)$$

alters into the Fourier convolution type transform

$$y(\omega_0 q^{\omega^*}) = \ln q\, x(\omega_0 q^{\omega^*}) * k(q^{\omega^*}) = \ln q \int_{-\infty}^{\infty} x(\omega_0 q^{u^*}) k(q^{\omega^* - u^*}) du^*,$$

which may be treated as an ideal convolution filter operating on the logarithmic domain.

Therefore, a discrete-time Mellin convolution filter operates with the data uniformly sampled in logarithmic domain (3) becoming geometrically sampled ones in the linear scale [8,9]

$$\omega_n = \omega_0 q^n, \quad n = 0, \pm 1, \pm 2, ..., \quad q > 1,$$

and executes discrete convolution algorithm

$$\tilde{y}(\omega_0 q^m) = h[n] * x(\omega_0 q^m) = \sum_n h[n] x(\omega_0 q^{m-n}), \quad (4)$$

where q is the common ratio for geometrically sampled data. The filter has a periodic frequency response [6-9]

$$H(e^{j\mu}) = \sum_n h[n] \exp(-j\mu \ln q) \quad (5)$$

in the Mellin transform domain and approximates the ideal frequency response, expressed by the Mellin transform of kernel $k(u)$ of MCT

$$H(j\mu) = M[k(u); -j\mu] = \int_0^{\infty} k(u) u^{-j\mu - 1} du, \quad (6)$$

where parameter μ, named the *Mellin frequency* [6,7], has a physical meaning as angular frequency for signals on the logarithmic domain.

Apart from typical computational problems of MCT [6-9], the separating magnitude response into the real and imaginary part poses several challenges. Although magnitude response (1) contains information about the real and imaginary parts, the operations of rising to the power and taking square root make that neither the real part nor the imaginary part can be related to magnitude response (1) through MCT, and hence, converting the magnitude response into the real and imaginary parts does not represent a Mellin filtering task.

An important matter common for all finite impulse response (FIR) filters is compensation of so-called *end effects* (named also *transient effects*) [10], which in the case of geometrically sampled data (magnitude responses) appear as an exponential shortening of frequency range of output signal (real and imaginary parts) [6].

The final purpose of this study was the construction of discrete-time magnitude-response-to-real-part transformers (further, *MR-to-Re transformers*) and magnitude-response-to-imaginary-part transformers (further, *MR-to-Im transformers*).

The rest of this paper is organized as follows. Theoretical background for separating the magnitude response into the real and imaginary parts by using Mellin convolution filters is given in Section 2. Implementation aspects including discrete-time transformer design and end-effect compensation for the real and imaginary parts are considered in Section 3. Simulation results and discussion are presented in Section 4, where performance evaluation and peculiar application features of designed transformers are described. Section 5 contains conclusions.

2 Theoretical Background

We will consider two limiting cases for magnitude response (1): (i) – when the imaginary part is small and tends to zero $J''(\omega) \to 0$, and (ii) – when the imaginary part takes the maximum value $J''(\omega) = J''_{\max}(\omega)$.

2.1 Limiting Case when Imaginary Part Tends to Zero

In this case, the magnitude response approaches to the real part $|\tilde{J}(\omega)| \to J'(\omega)$ allowing to estimate the imaginary part by the KK relation [1,11]

$$J''(\omega) \approx -\frac{2\omega}{\pi} \int_0^{\infty} \frac{|\tilde{J}(u)|}{u^2 - \omega^2} du, \quad (7)$$

while the real part may be taken approximately equal to the magnitude response

$$J'(\omega) \approx |\tilde{J}(\omega)|. \quad (8)$$

As shown in [11], KK relation (7) represents MCT with the following functions in the case of magnitude response (1): $x(\omega) = |\tilde{J}(\omega)|$, $y(\omega) = J''(\omega)$, and kernel

$$k''(u) = -2u/(1-u^2)/\pi,$$

which according to (6) gives the frequency response

$$H''_{\min}(j\mu) = M[k''(u); j\mu] = \tan(j\pi\mu/2). \quad (9)$$

In its turn, Eq. (8) may be treated as the determination of $J'(\omega)$ from $\left|\widetilde{J}(\omega)\right|$ by an all-pass filter with a constant (unit) frequency response

$$H'_{\min}(j\mu)=1. \quad (10)$$

2.2 Limiting Case with Maximum Imaginary Part

According to the phenomenological theories [12-14], the imaginary part of an elementary causal system with the monotonic IR has the following upper bound

$$J''_{\max}(\omega)=\frac{\Delta J\omega\tau}{1+\omega^2\tau^2} \quad (11)$$

with the corresponding real part

$$J'_{\max}(\omega)=\frac{\Delta J}{1+\omega^2\tau^2} \quad (12)$$

being consistent with KK relations [1,11]. The parts (12) and (11) give the following magnitude response

$$\left|\widetilde{J}_{\max}(\omega)\right|=\frac{\Delta J}{\sqrt{1+\omega^2\tau^2}}, \quad (13)$$

where ΔJ is factor of proportionality while τ is characteristic time of the system.

Nevertheless, magnitude response (13) is not often adequate for real systems, such as materials [12-14], because the real parts of materials contain, as a rule, constant instantaneous values. Hence, we consider the real part with added constant J_∞

$$J'_{\max}(\omega)=J_\infty+\frac{\Delta J}{1+\omega^2\tau^2}. \quad (14)$$

Then the parts (14) and (11) create a magnitude response

$$\left|\widetilde{J}_{\max}(\omega)\right|=\sqrt{\left(J_\infty+\frac{\Delta J}{1+\omega^2\tau^2}\right)^2+\left(\frac{\Delta J\omega\tau}{1+\omega^2\tau^2}\right)^2}=\sqrt{J_\infty^2+\frac{2\Delta JJ_\infty}{1+\omega^2\tau^2}+\frac{\Delta J^2}{1+\omega^2\tau^2}} \quad (15)$$

which does not represent MCT in regard to the parts (14) and (11). Based on (13), we propose to approximate magnitude response (15) by a Mellin convolution transformable function

$$A(\omega)=\sqrt{J_\infty^2+\frac{2\Delta JJ_\infty}{\sqrt{1+\omega^2\tau^2}}+\frac{\Delta J^2}{1+\omega^2\tau^2}}=J_\infty+\frac{\Delta J}{\sqrt{1+\omega^2\tau^2}},$$

which slightly overestimates response (15).

Contrary to the functions of pairs $\left\{J'_{\max}(\omega),\left|\widetilde{J}(\omega)\right|\right\}$ and $\left\{J''_{\max}(\omega),\left|\widetilde{J}(\omega)\right|\right\}$, the functions of pairs $\left\{J'_{\max}(\omega),A(\omega)\right\}$ and $\left\{J''_{\max}(\omega),A(\omega)\right\}$ may be related to each other in terms of the Mellin transforms

$$M\left[J'_{\max}(\omega);-j\mu\right]=M\left[A(\omega);-j\mu\right]\cdot H'_{\max}(j\mu); \quad (16)$$

$$M\left[J''_{\max}(\omega);-j\mu\right]=M\left[A(\omega);-j\mu\right]\cdot H''_{\max}(j\mu), \quad (17)$$

where $H'_{\max}(j\mu)$ and $H''_{\max}(j\mu)$ are frequency responses of MR-to-Re and MR-to-Im transformers in the limiting case with the maximum imaginary part. To take into account (16) and (17), frequency responses $H'_{\max}(j\mu)$ and $H''_{\max}(j\mu)$ may be determined as follows

$$H'_{\max}(j\mu)=M\left[J'_{\max}(\omega);-j\mu\right]/M\left[A(j\mu);-j\mu\right];$$

$$H''_{\max}(j\mu)=M\left[J''_{\max}(\omega);-j\mu\right]/M\left[A(j\mu);-j\mu\right].$$

By using the Mellin transforms

$$M\left[J'_{\max}(\omega);-j\mu\right]=\frac{\pi}{2}\frac{\Delta J}{\sin(-j\pi\mu/2)};$$

$$M\left[J''_{\max}(\omega);-j\mu\right]=\frac{\pi}{2}\frac{\Delta J}{\cos(j\pi\mu/2)};$$

$$M\left[A(j\mu);-j\mu\right]=\frac{2^{-j\mu}\Gamma(2+j2\mu)\Gamma(-j\mu)\Delta J}{\Gamma(2+j\mu)},$$

the following frequency responses were obtained for the MR-to-Re and MR-to-Im transformers in the limiting case with maximum imaginary part:

$$H'_{\max}(j\mu)=\frac{\pi\Gamma(2+j\mu)}{2^{1-j\mu}\Gamma(2+j2\mu)\Gamma(-j\mu)\sin(-j\pi\mu/2)}; \quad (18)$$

$$H''_{\max}(j\mu)=\frac{\pi\Gamma(2+j\mu)}{2^{1-j\mu}\Gamma(2+j2\mu)\Gamma(-j\mu)\cos(j\pi\mu/2)}, \quad (19)$$

where $\Gamma(.)$ is gamma function.

2.3 Diffuse Magnitude Responses

In Fig. 1(a), functions $|H'_{\min}(j\mu)|$ and $|H'_{\max}(j\mu)|$ are shown, which form the bounds for the magnitude response of an ideal MR-to-Re transformer, while in Fig. 1(b), functions $|H''_{\min}(j\mu)|$ and $|H''_{\max}(j\mu)|$ are demonstrated, which also create the bounds of the magnitude response for an ideal MR-to-Im transformer. Depending on the values for the real and imaginary parts, MR-to-Re and MR-to-Im transformers have different ideal magnitude responses $|H(j\mu)|$, but all they must be located within the indicated above bounds. Therefore, ideal MR-to-Re and MR-to-Im transformers may be treated as Mellin convolution filters with *diffuse* magnitude responses.

At low Mellin frequencies $|\mu|<0.5$, MR-to-Im transformer has a united – not diffused – magnitude response. This indicates actually on a practical feasibility of using KK transformers [11] for estimating the imaginary part from the magnitude response. An important point is that MR-to-Im transformer has zero frequency response at zero frequency $H''(j0)=0$, which ensures cutting out zero frequency component (DC component) of an input magnitude response and, thus, minimizes the effect of constant J_∞.

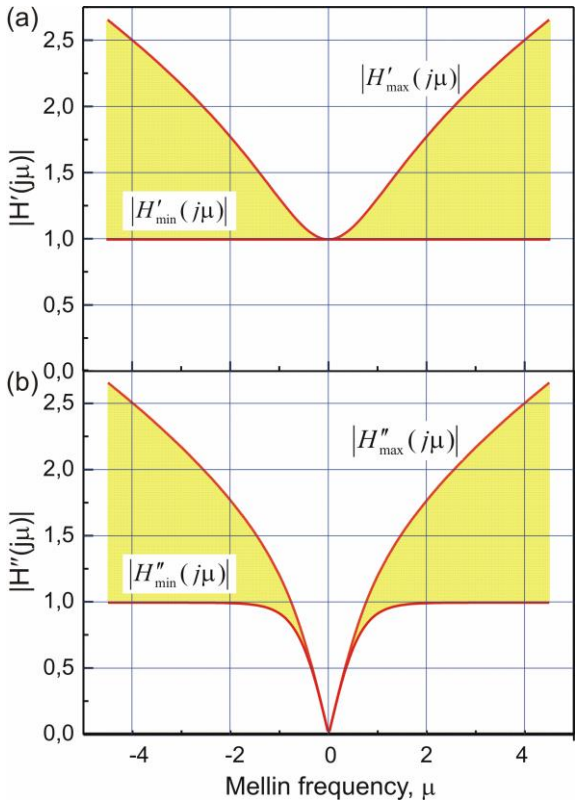

Fig. 1. Diffuse magnitude responses of ideal MR-to-Re (a) and MR-to-Im (b) transformers.

3 Implementation Aspects

3.1 Design of Discrete-Time Transformers

Based on classification of MR-to-Re and MR-to-Im transformers as Mellin convolution filters with diffuse magnitude responses, we designed the discrete-time transformers in the form (4) by the learning to use the system identification principle [6,7] with pairs of the exact functions $\left\{J'(\omega),\left|\widetilde{J}(\omega)\right|\right\}$ and $\left\{J''(\omega),\left|\widetilde{J}(\omega)\right|\right\}$ corresponding to the Cole-Cole model [16]. Taking into account our experience with the development of discrete-time KK transformers [11], we used the same common ratio $q=2$ and filter length $N=8$. It is important to stress that the design of the transformers has been performed in input-output signal domain without involving the diffuse frequency responses, i.e. bounds (10) and (18), as well as (9) and (19).

3.2 End-Effects Compensation

As it is known [6,10], FIR filters suffer from of the end effects problem, in particular, in processing aperiodic signals, appearing as shortening usable filtered sequences in the beginning and end. Since the full overlapping of a portion of input signal with IR must be provided requiring that *N* input samples without zeros must be convolved with the filter coefficients to compute a correct output sample, a FIR filter allows obtaining only a correct output sequence, which is by $N-1$ samples shorter than input sequence. This shortening is particularly undesirable for geometrically sampled datasets [6,11,15], because exponentially – by q^{N-1} times – reduces dynamic interval (range) of independent variable for output waveform to compare with the dynamic interval (range) of independent variable for input function. The common ratio $q=2$ and filter length $N=8$ used here shorten dynamic frequency range for the real and imaginary parts $q^{N-1}=2^7=128$ times.

To overcome this drawback, we use the multiple filtering mode [6,11,15] for the first and last *N* input samples, when instead of the traditional sliding filtering mode [2], where a single IR moves along the input sequence, the origins of fixed (non-moved) IRs move along the input sequence. To realize the multiple filtering mode, we designed additional filters, where the origins of IRs were shifted the left and right in regard to the origin of the non-shifted IR of the sliding mode filter to attain

gradual variation of the number of coefficients with negative and positive indices on each side of the origin. We designed the additional filters with the shifts of IRs altering by step 0.5, to provide the expansion of the frequency range for the real and imaginary parts together with doubling the sampling rate ($q_y = \sqrt{2} = 1.41$). The designed filters were combined in filter banks [6].

4 Simulation Results and Discussion

4.1 Performance Evaluation

Following the suggestion in [6,11,15], we evaluated the performance of discrete-time transformers by: (i) accuracy of the generated real and imaginary parts and (ii) noise amplification of the transformers.

The accuracy was determined by a difference (error) between computed output $\hat{y}(\omega)$ and exact (true) output $y(\omega)$

$$e(\omega) = \hat{y}(\omega) - y(\omega),$$

which was quantitatively estimated by mean-square error (MSE)

$$E = (1/M)\sum_{m=1}^{M} e^2(\omega_m). \quad (20)$$

As true waveforms $y(\omega)$, we use the exact real and imaginary parts corresponding to the Havriliak-Negami model [17] with the following frequency response

$$\tilde{J}(\omega) = J_\infty + \Delta J\left[1 + (j\omega\tau)^\alpha\right]^{-\beta}. \quad (21)$$

The model (21) allows to change shapes of the real and imaginary parts, and, consequently, the magnitude responses to large extent to vary parameters α, β, J_∞ and ΔJ. In this study, we calculate error (20) for $M = 100$ points of the real and imaginary parts equally spaced on the logarithmic frequency domain over the frequency range $10^{-5} \le \omega \le 10^5$ at characteristic time $\tau = 1$.

In its turn, noise amplification was quantitatively estimated by noise gain (amplification coefficient) [6]

$$S = \sum_n h^2[n],$$

showing how the noise variance σ_x^2 of input data (magnitude response) is transmitted to the noise variance σ_y^2 of the output data (real and imaginary parts) $\sigma_y^2 = S\sigma_x^2$.

4.2 Sliding Mode Transformers

In Table, the coefficients are given for basic – sliding mode MR-to-Re and MR-to-Im transformers with non-shifted IRs having 4 coefficients with negative and positive indices on each side of the origin of IR. It can be seen that the transformers are non-linear phases filters [2] having the coefficients with no symmetry.

Table. Coefficients for MR-to-Re and MR-to-Im transformers

n	**Coefficients *h*[*n*]**	
	MR-to-Re transformer	**MR-to-Im transformer**
-3.5	-0.00862702	0.109042
-2.5	0.0474832	0.0134620
-1.5	-0.143979	0.165268
-0.5	0.480793	0.601015
0.5	0.759683	-0.372957
1.5	-0.185825	-0.470905
2.5	0.0656697	0.136201
3.5	-0.0153284	-0.178838

In Figs. 2 and 3, as examples, the exact real and imaginary parts (solid) and the computed ones (dashed) by the designed transformers are shown for $\beta = 1$ and $\beta = 0.5$, and five values of α to keep constant parameters $J_\infty = 3$, and $\Delta J = 1$. The chosen values for the parameters are close to those used for describing complex dielectric permittivity of typical polymers [13,14].

As seen, the accuracy of computing the real and imaginary parts is quite high, particularly, for the real parts at $\beta = 0.5$, where it is hard to distinguish between the exact and computed curves.

4.3 Transformer Banks

Shifts of the origins of IRs have typically adverse effect on the performance to increase of both MSEs and the noise gains. In this study, we limited the performance with MSEs $E \le 0.5$ and the noise gain $S \le 20$. Within these limitations, we constructed a bank consisting of 17 MR-to-Re transformers covering the shift interval over $-4 \le s \le 4$ and a bank of 10 MR-to-Im transformers covering the shift interval over $-2 \le s \le 2.5$.

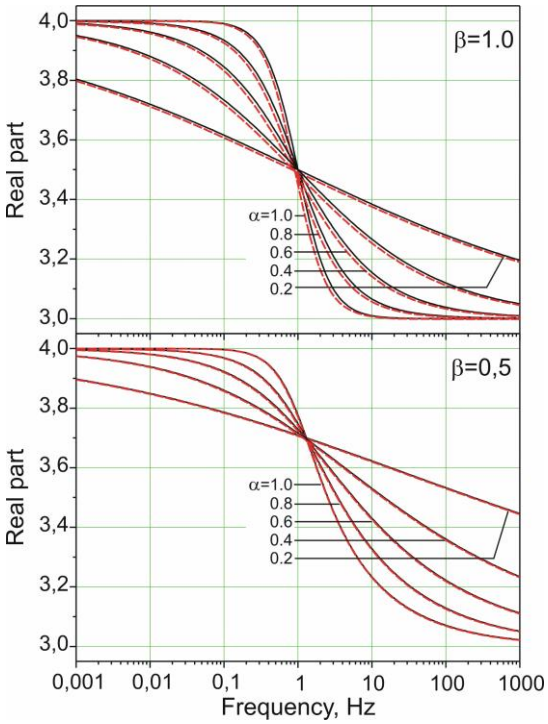

Fig. 2. Exact (solid) and computed (dashed) real parts.

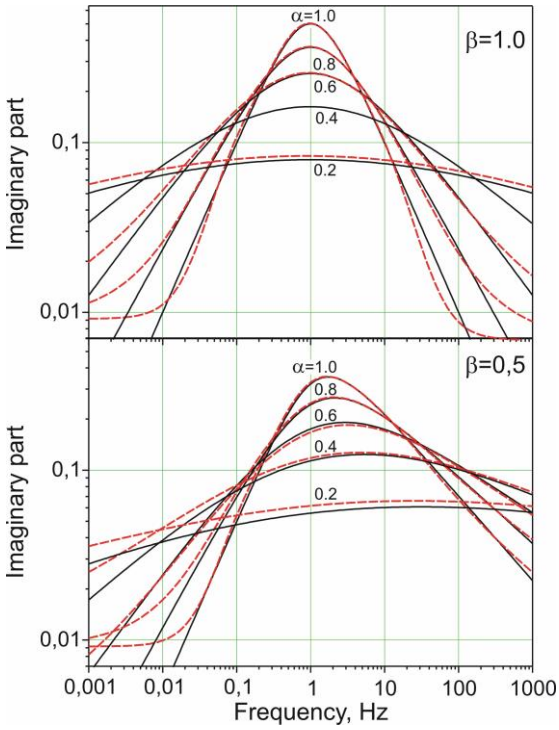

Fig. 3. Exact (solid) and computed (dashed) imaginary parts.

In Fig. 4, MSEs are shown as functions of the shifts of the origins of IRs for transformers of the constructed banks calculated for combinations ($\alpha = 1, \beta = 1$) and ($\alpha = 0.5, \beta = 0.5$) and the fixed parameters $J_\infty = 3$, and $\Delta J = 1$. Similarly, the noise gains of transformers are shown in Fig. 5 for the both banks.

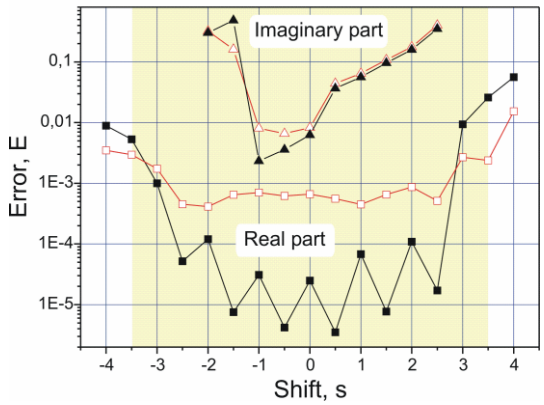

Fig. 4. Variation of MSE from the shift. Solid symbols: $\alpha = 1$, $\beta = 1$, open symbols: $\alpha = 0.5$, $\beta = 0.5$. Shaded area: the shift interval necessary for covering the frequency range of the magnitude response for $N = 8$.

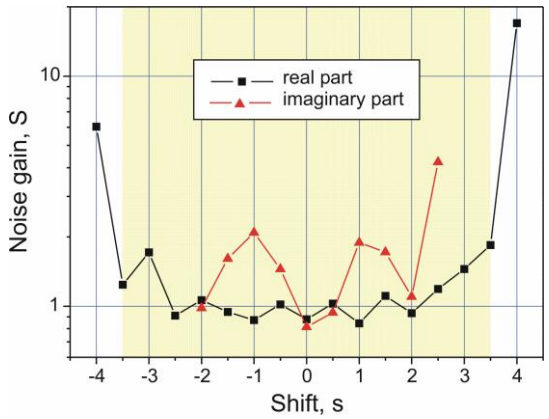

Fig. 5. Variation of the noise gain from the shift. Shaded area: the shift interval necessary for covering the frequency range of the magnitude response for $N = 8$.

As it is seen, the real part is determined with the higher accuracy over the wider frequency range compared with the imaginary part. The constructed MR-to-Re transformer bank allows to cover frequency range from $2^{-0.5} f_{\min}$ to $2^{0.5} f_{\max}$ providing two times larger dynamic frequency range than that of the magnitude response $f_{\max} / f_{\min}$. Therefore, MR-to-Re transformers with the maximum shifts $s = \pm 4$ determine the real part outside the frequency range of the measured magnitude response, i.e. work as extrapolators. However, these transformers may

be impracticable due to increased noise gains (see Fig. 7).

In its turn, the constructed MR-to-Im transformer bank allows to determine the imaginary part within frequency range from $2^{1.5}f_{\min}$ to $2^{-1}f_{\max}$, i.e. over dynamic frequency range that is $2^{2.5} \approx 5.66$ times narrower than that of the measured magnitude response.

4.4 Behaviour in the Mellin Frequency Domain

In Fig. 6(a), the magnitude responses are shown for MR-to-Re transformers with zero and ±0.5 shifts of the origins of IRs. As it is seen, the magnitude responses are well fitted to the magnitude response (10) of the ideal all-pass filter. It is interesting to note that just the transformers with shifts $s = \pm 0.5$, and not the transformer with zero shift, have the better fit and the higher accuracy for symmetric real parts ($\alpha = 1, \beta = 1$) (see Fig. 4) .

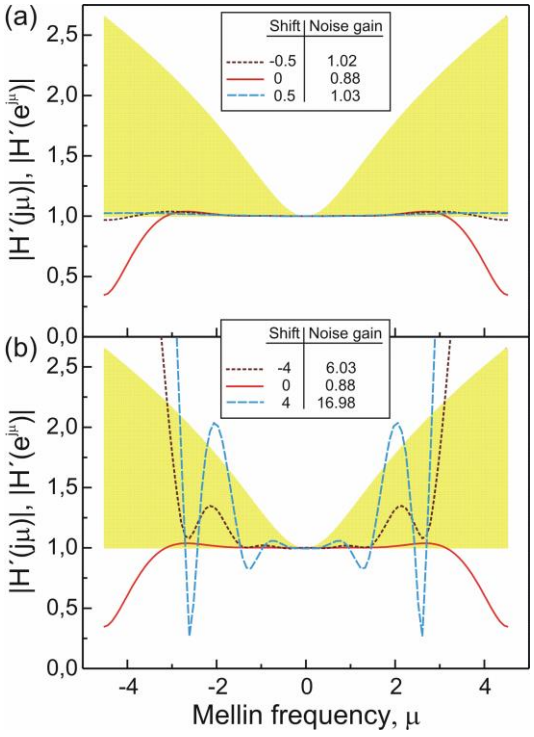

Fig. 6. Magnitude responses of MR-to-Re transformers with different shifts. Shaded area: ideal diffuse magnitude response.

In general, within the interval of the shift $|s| \le 2.5$, MR-to-Re transformers have relatively smooth magnitude responses, which according to the Parseval's relation [2] result in relatively low noise gains, which oscillate around value 1 (see Fig. 5) and have the mean value $\bar{S} = 0.96$. The shifts either to the left and right greater than 2.5 produce substantially larger lateral lobes, which have adverse effect on the accuracy of generated waveforms and increase noise amplification. Enormous lateral lobes arise for the extrapolation transformers with $s = \pm 4$ (Fig. 6(b)), which are accompanied by large noise gains (see Fig. 5). The simulations performed showed that, just the noise gain, not the accuracy, typically limits the expansion of frequency range in the multiple filtering mode.

The behaviour of MR-to-Im transformers are similar to that described above. For the imaginary parts, the larger variations are observed in the magnitude responses causing larger dispersions in the noise gains (see Fig. 5). As an example, in Fig. 7, the magnitude responses are shown for zero and maximum shifts. It is seen, that tremendous lateral lobe is produced at the shift $s = 2.5$.

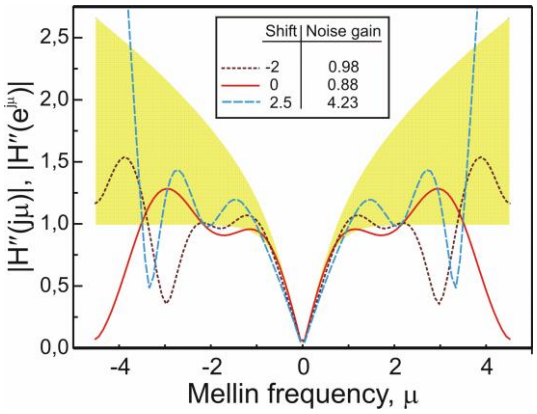

Fig. 7. Magnitude responses of MR-to-Im transformers with different shifts. Shaded area: ideal diffuse magnitude response.

5 Conclusions

We have demonstrated that a problem of separating the magnitude response into the real and imaginary parts for causal linear time-invariant systems may be considered in filtering framework in the Mellin transform domain with diffuse frequency responses, which establishes a theoretical foundation for the determination of the real and imaginary parts by discrete-time Mellin convolution filters processing geometrically sampled magnitude responses. Discrete-time magnitude-response-to-real-part and magnitude-response-to-imaginary-part transformers have been designed in the form of FIR Mellin convolution filters.

To overcome exponential shortening frequency ranges of the real and imaginary parts due to the end-

effects of FIR filters operating with geometrically sampled magnitude responses, we have used the multiple filtering mode by repeated processing sets of the first and last *N* input samples by the transducers having impulse responses with the shifted origins, which gradually vary the number of coefficients with negative and positive indices on each side of the origin. Transformer banks have been constructed for implementing the multiple filtering mode.

We have evaluated performance of the transformers in terms of the accuracy of the generated real and imaginary parts and the noise gain of the transformers. It has been found that the real part can be determined with the higher accuracy over wider frequency range compared with the imaginary part.

We have disclosed that increased shifts of the origins of impulse responses produce lateral lobes in the appropriate magnitude responses of the Mellin convolution filters, which enlarge the noise gains and reduce the accuracy of the generated real and imaginary parts, and just the enlargement of the noise gain is the main factor limiting expansion of frequency ranges in the multiple filtering mode.

Acknowledgements

This work was supported by the European Regional Development Fund under project No. 1.1.1.1/16/A/008.

References:

[1] H.M. Nussenzveig, *Causality and Dispersion Relations*; Academic Press, 1972.

[2] A.V. Oppenheim, R.V. Schafer, *Discrete-Time Signal Processing*, Sec. Ed., Prentice-Hall International, 1999.

[3] V. Strauss, A. Kalpins, U. Lomanovskis, Method and device for estimating the real and imaginary parts of the frequency response, *Patent WO2015047065A1*, 2013.

[4] V. Shtrauss, A. Kalpinsh, Determination of relaxation and retardation spectrum from modulus of complex frequency-domain material functions, *WSEAS Transactions on Applied and Theoretical Mechanics*, Vol. 7, Issue 1, 2011, pp. 29-38, http://www.wseas.org/multimedia/journals/mechanics/2012/54-080.pdf .

[5] A. Kalpinsh, V. Shtrauss, Measurement systems for distribution of relaxation and retardation times, *Proc. 15th WSEAS International Conference on Systems RECENT RESEARCHES in SYSTEM SCIENCE*, Corfu Island, Greece, July 14-16, 2011, pp. 106-111, http://www.wseas.us/e-library/conferences/2011/Corfu/SYSTEMS/SYSTEMS-15.pdf .

[6] V. Shtrauss, Digital interconversion between linear rheologic and viscoelastic material functions. In: *Advances in Engineering Research.* Vol. 3, Ed. V.M. Petrova, Nova Science Publishers, 2012, pp. 91-170, https://www.novapublishers.com/catalog/product_info.php?products_id=34008 .

[7] V. Shtrauss, Digital signal processing for relaxation data conversion, *Journal of Non-Crystalline Solids*, Vol. 351, 2005, pp. 2911-2916.

[8] V. Shtrauss, Sampling and algorithm design for relaxation data conversion, *WSEAS Transactions on Signal Processing*, Vol. 2, 2006, pp. 984-990.

[9] V. Shtrauss, Sampling in Relaxation Data Processing, *Proceedings of the 10th WSEAS International Conference on SYSTEMS*, Vouliagmeni, Athens, Greece, July 10-12, 2006, pp. 37-42.

[10] A. Arguez, P. Yu, J.J. O'Brien, A new method for time series filtering near endpoints, *J. Atmos. Oceanic Tech.*, Vol. 25, 2008, pp. 534-546.

[11] V. Shtrauss, FIR Kramers-Kronig transformers for relaxation data conversion, *Signal Processing,* Vol. 86, 2006, pp. 2887-2900.

[12] J.D. Ferry, *Viscoelastic Properties of Polymers*, 3rd. ed., J. Wiley and Sons, 1980.

[13] N.G. McCrum, B.E. Read, G. Wiliams, *Anelastic and Dielectric Effects in Polymer Solids*, J. Wiley and Sons, 1967.

[14] A.K. Jonscher, *Dielectric Relaxation in Solids*, Chelsea Dielectric, 1983.

[15] V. Shtrauss, Recovery of relaxation and retardation spectra over expanded intervals with increased density of spectrum points, *Mathematical Applications in Science and Mechanics. Proc. 9th International Conference on Applied and Theoretical Mechanics* (MECHANICS'13), Dubrovnik, Croatia, June 25-27, 2013, p. 21-26,

[16] K.S. Cole, R.H. Cole, Dispersion and absorption in dielectric. Alternating current characteristics, *J. Chem. Phys*., Vol. 9, 1941, pp. 341-351.

[17] S. Havriliak, S.J. Havriliak, A complex plane representation of dielectric and mechanical relaxation processes in some polymer, *Polymer* 1967, *8,*161-210.